Accepted Manuscript

Amperometric Sarcosine Biosensor Based on Hollow Magnetic Pt-Fe_3O_4@C Nanospheres

Qingui Yang, Na Li, Qiang Li, Shaoqing Chen, Hsing-Lin Wang, Haipeng Yang

PII: S0003-2670(19)30756-1

DOI: https://doi.org/10.1016/j.aca.2019.06.031

Reference: ACA 236873

To appear in: *Analytica Chimica Acta*

Received Date: 28 May 2019

Revised Date: 9 June 2019

Accepted Date: 10 June 2019

Please cite this article as: Q. Yang, N. Li, Q. Li, S. Chen, H.-L. Wang, H. Yang, Amperometric Sarcosine Biosensor Based on Hollow Magnetic Pt-Fe_3O_4@C Nanospheres, *Analytica Chimica Acta*, https://doi.org/10.1016/j.aca.2019.06.031.

Graphical Abstracts

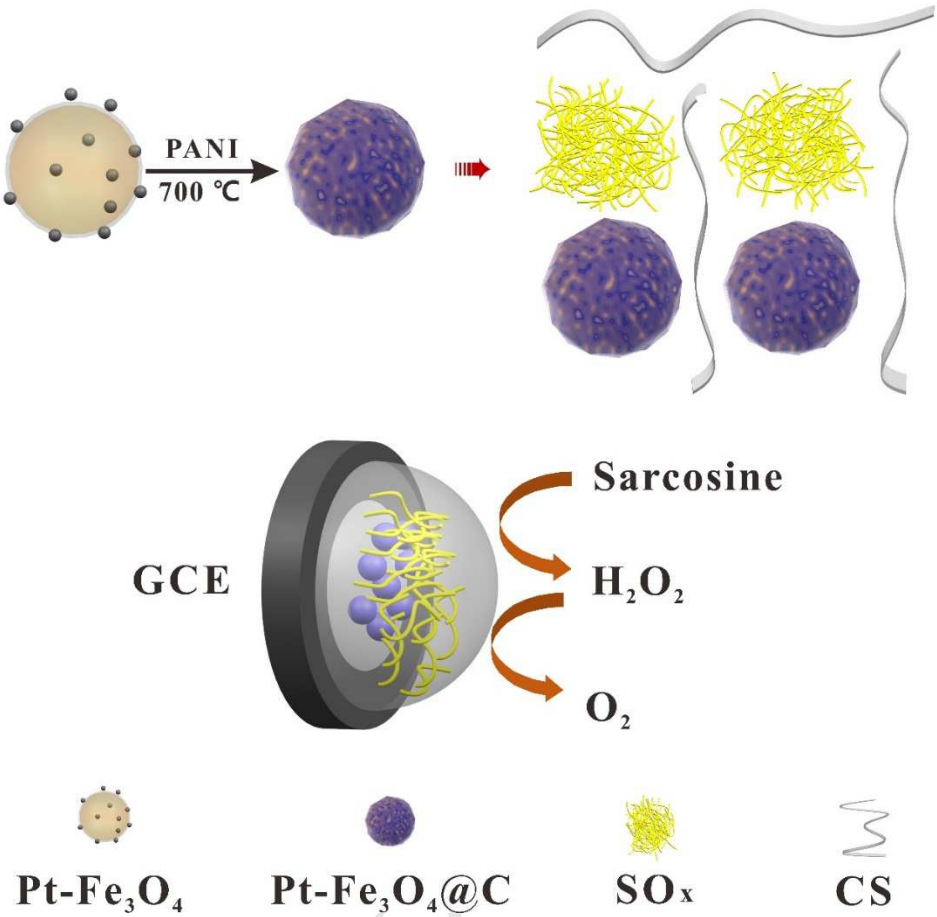

Amperometric Sarcosine Biosensor Based on Hollow Magnetic Pt-Fe_3O_4@C Nanospheres

Qingui Yang[a], Na Li[a], Qiang Li[a], Shaoqing Chen[b], Hsing-Lin Wang[b], Haipeng Yang[a] *

[a.] College of Materials Science and Engineering, and Shenzhen Key Laboratory of Polymer Science and Technology, Shenzhen University, Shenzhen, 518060, China;

[b.] Department of Materials Science and Engineering, Southern University of Science and Technology, Shenzhen 518055, P.R. China

Abstract

Sarcosine is a recently identified biomarker for prostate cancer. However, the rapid detection methods for sarcosine are relatively lack because of the low concentration and the presence of complicated interfering substances in serum or urine. In this manuscript, hollow nanospheres of Fe_3O_4 was synthesized and used as carrier to disperse Pt (Pt) nanoparticles. In order to achieve excellent electron transfer ability, we use polyaniline to coat Pt-Fe_3O_4 nanoparticles, and pyrolyze the polyaniline to carbon (C). Thus, hollow magnetic Pt-Fe_3O_4@C nanocomposites with good electron transfer ability are formed. The Pt-Fe_3O_4@C nanocomposites have high catalytic activity and stability. The nanocomposites were immobilized on glassy carbon electrode (GCE) to construct a nonenzyme hydrogen peroxide (H_2O_2) sensor (Pt-Fe_3O_4@C/GCE). We further construct a sensitive sarcosine biosensor by immobilizing sarcosine oxidase (SOx) on the Pt-Fe_3O_4@C/GCE. The high catalytic activity and good biocompatibility of Pt-Fe_3O_4@C nanocomposites greatly retained the bioactivity of immobilized SOx, and the prepared sarcosine biosensor has good electrocatalytic performance towards sarcosine. It has a linear detection range between 0.5-60 μM with a limit of detection (LOD) of 0.43 μM (the signal to noise ratio is 3), and the sensitivity is 3.45 nA μM^{-1} (48.8 nA μM^{-1} cm^{-2}), which has the potential to be used for rapid screening of prostate cancer.

Key words: Biosensor; Electrochemical Sensor; Sarcosine; Prostate Cancer; Nanosphere

1. Introduction

Corresponding author Tel: +86 755 86713943, *E-mail address*: yanghp@szu.edu.cn;

Sarcosine has been identified as a differential metabolite whose concentration in serum or urine is highly elevated during prostate cancer progression[1]. Therefore, sarcosine may become a sensitive biomarker for the prostate cancer screen. However, the quantitative determination of sarcosine is particularly difficult due to the very low concentration and the presence of complicated interfering substances in serum or urine. In most cases, quantitative detection of sarcosine is usually achieved by mass spectrometry (MS) based methods[2-4]. However, these methods are not suitable for routine detection because of the high cost, the difficulty of instrument operation and sample preparation. Biosensors have the properties of simple and inexpensive[5-7]. The most popular way to detect enzyme reactions in various biosensors is to monitor the production of enzymatic catalytic reactions. In the presence of oxygen, sarcosine is catalyzed by sarcosine oxidase (SOx) to produce formaldehyde, glycine and hydrogen peroxide (H_2O_2)[8, 9]. On the other hand, H_2O_2 plays an important role in many fields such as the medicine, chemical synthesis, textile, environmental protection and food[10-14]. Compared with other methods for the detection of H_2O_2, electrochemical sensors have attracted wide attention for their rapid, economical, accurate and reliable quantitative analysis[15]. In this work, the concentration of H_2O_2 is proportional to the concentration of sarcosine. Therefore, the determination of sarcosine could be realized by electrochemical detection of H_2O_2. The chemical equation (1) and (2) shows the enzymic catalytic reaction and the electro-catalytic reaction[16].

$$\text{Sarcosine} + H_2O + O_2 \xrightarrow{\text{SOx}} \text{Formaldehyde} + \text{Glycine} + H_2O_2 \quad (1)$$

$$H_2O_2 \xrightarrow{0.3\ \text{V}} O_2 + 2H^+ + 2e^- \quad (2)$$

Based on an electrochemical H_2O_2 sensor, some sensitive sarcosine biosensors had been constructed successfully, which provides a more convenient diagnosis method for prostate cancer screening[6, 9, 17, 18]. Though the previously reported sarcosine biosensors have their advantages, there are still many work to do to improve the detection performance. In Rebelo's work, the linear range of sarcosine biosensor is very well (0.01-0.1 μM). However, it does not refer to the anti-interference property of ascorbic acid (AA), uric acid (UA) or dopamine (Dop)[16]. In Pundir's work, both the linear range and the anti-interference property of sarcosine biosensor is fairly well. However, this work use gold electrode and with a high applied voltage of 1 V vs Ag/AgCl[19].

Rebelo's work has showed that the anti-interference property of gold electrode is not satisfied even at a lower voltage (0.6 V)[16]. So the reason of its good anti-interference property is worthy of further studies, especially under such a high voltage. Much more work is worthy to do since sarcosine is a better biomarker for prostate cancer.

Magnetic Fe_3O_4 nanomaterial has the properties of superparamagnetic, good biocompatibility, low toxicity, easy to prepare, and easy to be functionalized. It has been widely used in environmental detection, electrochemistry, biomedical, medical diagnosis and medicine[20-24]. The properties and applications of Fe_3O_4 nanoparticles depend on their crystallinity, size and morphology, especially the size effect of nanoparticles[25, 26]. Fe_3O_4 is a multifunctional magnetic recycling heterogeneous supporter which can be used as a carrier for the preparation of versatile catalysts[27]. Precious metal nanomaterials have received extensive attention because of their excellent performances in the fields of optics, magnetism, electricity, and catalysis[18, 28-30]. However, due to the limitations of their properties and rare reserves, the large-scale application of precious metal nanomaterials have been greatly limited. Therefore, it is desirable to reduce the use of precious metals while improving composited with other non-precious metals[31, 32]. Its physical and chemical properties such as optical, electrical, magnetic, catalytic, and mechanical properties can be significantly altered by controlling size, morphology, and structure[33-36]. In this study, Fe_3O_4 hollow nanospheres werefabricated and used as carrier to support platinum (Pt), and further was combined with carbon (Pt-Fe_3O_4@C) to achieve good conductivity. The Pt-Fe_3O_4@C nanocomposite makes full use of the three materials (precious metal, magnetic material, and conductive material) and shows very high electrocatalytic activities. In addition, the Pt-Fe_3O_4@C nanocomposites also greatly reduce the amount of Pt (only 1.1 wt%) compared with other Pt biosensors[18, 28-30]. This indicates that this nanocomposites can provide more active sites. The prepared enzyme free H_2O_2 sensor and the sarcosine biosensor have a rapid and sensitive response to H_2O_2 and sarcosine, respectively. Because of the sarcosine biosensor has a very low limit of detection (LOD), it is suitable to be used in the large-scale screening of prostate cancer. The Pt-Fe_3O_4@C nanocomposites also have potential use to construct biosensors for other low concentration substrates in the field of food safety and medical, etc.

2 Material and methods

2.1 Reagents and instruments

SOx got from J&K Scientific Ltd (lyophilized powder, 25 U.mg^{-1}). The SOx solution (1 U. μL^{-1}) was prepared by dissolving SOx in sodium phosphate buffer (PBS, pH 7.0) which contains 7% bovine serum albumin (BSA). Sarcosine was purchased from Shanghai Macklin Biochemical Co., Ltd. Chitosan (CS) was purchased from Sigma-aldrich Co., Ltd.. H_2O_2 was obtained from Shanghai Aladdin Biochemical Technology Co., Ltd. (30 wt%). The serum sample was purchased from Huayang Zhenglong Biochemical Products Laboratory. Ultra-pure water (18.2 MΩ•cm^{-1}) was used in this work.

Scanning electron microscope (SEM) was conducted by using S-4800 scanning electron microscope. Transmission electron microscope (TEM) observations were carried out on a Joel 2100F apparatus equipped with an energy-dispersive X-ray spectrometer (EDS). Electrochemical measurements data were recorded by CHI660E electrochemical workstation (Shanghai, China). All the electrochemical experiments were implemented with a three electrode system. In the three electrodes system, the reference electrode was saturated calomel electrode (SCE), meanwhile the auxiliary electrode and the working electrode were composed of Pt electrode and modified glassy carbon electrode (GCE), respectively.

2.2 Preparation of Pt-Fe_3O_4@C nanocomposites

The Fe_3O_4 hollow nanospheres wereprepared by hydrothermal method. $FeCl_3 \cdot 6H_2O$ (1.35 g) and ammonium acetate (3.85 g) was dissolved in 70 mL of ethylene glycol, magnetically stirred for 0.5 h, and the mixed solution was placed in an autoclave and kept at 200 °C for 8 h[37]. After cooling to room temperature for several hours, the upper layer clarified solution was separated. The black sediment was centrifuged (10000 rmp, 4 min) and washed with ethanol and dried in a vacuum drying oven at 60 °C for 10 h. The obtained black powder was Fe_3O_4 hollow nanospheres. The nano Pt was loaded on the Fe_3O_4 hollow nanospheres by thermal reduction method. 5 mL of $H_2PtCl_6 \cdot 6H_2O$ solution (0.02 g·mL^{-1}) was used to soak Fe_3O_4 nanospheres for 48h. Then the nanospheres weredried in a vacuum drying oven at 60 °C for 10 h. The dried nanospheres weresintered at 500 °C for 5 h to obtain Pt-Fe_3O_4 composite nanoparticles. 0.15 g Pt-Fe_3O_4 was dispersed in 15 mL ethanol solution that containing 4 mL of aniline, and certain amount of $FeCl_3 \cdot 6H_2O$ was dissolved in 5 mL ethanol

solution. The above two kinds of solution were mixed with ultrasonication for about 60 min to polymerize aniline and form polyaniline (PANI). The mixed solution was finally centrifuged to obtain Pt-Fe_3O_4@PANI nanocomposites, and the nanocomposites weredried in a vacuum drying oven at 60 °C for 10 h. Then the Pt-Fe_3O_4@PANI nanocomposites was calcined at 700 °C under Ar atmosphere to carbonize the PANI to form the nanocomposites of Pt-Fe_3O_4@C.

2.3 Fabrication of modified electrode and sarcosine biosensor

The bare glassy carbon electrode (GCE, Ø3 mm) were polished with Al_2O_3 powder (0.3 μm) to a mirror surface, washed with ultra pure water, soaked in anhydrous ethanol for 5 min and then dried naturally. The Pt-Fe_3O_4@C electrode (Pt-Fe_3O_4@C/GCE) was obtained by dropping 10 μL turbid solution on the surface of the modified electrode. The turbid solution was composed of 10 mg of Pt-Fe_3O_4@C nanocomposites, 0.04 mL of 1% CS, 0.21 mL of ethanol and 0.75 mL of water. The mixed solution was ultrasonicated for 2 h. For comparison, the Fe_3O_4/GCE, Pt-Fe_3O_4/GCE and Pt-Fe_3O_4@PANI/GCE were also prepared by using Fe_3O_4, Pt-Fe_3O_4 or Pt-Fe_3O_4@PANI nanoparticles according to the same procedure.

The SOx/Pt-Fe_3O_4@C/GCE sarcosine biosensor was fabricated by dripping 4 μL of 1 $U{\cdot}\mu L^{-1}$ SOx solution onto the surface of Pt-Fe_3O_4@C/GCE and dried 2 h at room temperature, then coated with 4 μL of 1% CS. After it was dried naturally, the sarcosine biosensor was successfully prepared.

The fabrication process and the mechanism of the sarcosine biosensor is schematically shown in scheme 1.

Scheme 1

3. Results and Discussion

3.1 Characterization of the Pt-Fe_3O_4@C

Fe_3O_4 hollow nanospheres wereprepared mainly according to the reported literature[37]. The nano Pt was loaded on the Fe_3O_4 nanospheres to obtain Pt-Fe_3O_4 composite by thermal reduction method. Pt-Fe_3O_4@PANI nanocomposites wereprepared by polymerizing aniline monomer into polyaniline with the catalytic action of Fe^{3+}. At last, the Pt-Fe_3O_4@PANI was calcined at 700 °C under Ar atmosphere to form the Pt-Fe_3O_4@C nanocomposites. The final Pt-Fe_3O_4@C was characterized by

SEM and TEM. As shown in Fig.1a, the Pt-Fe_3O_4@C shows a spherical structure with a uniform outer diameter of several hundred nanometers. Pt particles with a diameter of about 3-7 nm can be found on the surface of the hollow spheres (Fig. 1b). The hollow spheres are confirmed by TEM (Fig. 1c). The element mapping (Fig. 1d) shows that the C and Pt elements are uniformly dispersed on the sphere, showing the uniformly distribution of Pt nanoparticles. The element analysis spectrum shows the existence of Pt (1.1 wt%) and Fe (87.9 wt%) (Fig. 1e). The relative low content of Pt indicates the high dispersion of Pt nanoparticles[38]. The selected area electron diffraction pattern (Fig. 1f) is a polycrystalline ring pattern, which belongs to the Pt-Fe_3O_4 nanocomposites. These results indicate the successful preparation of Pt-Fe_3O_4@C nanocomposites and the uniformly distribution of nano Pt.

[Fig. 1]

3.2 Electrochemical performance of the modified electrode

In order to study the potential applications of Pt-Fe_3O_4@C nanomaterials in the field of electrochemical analysis, an electrochemical non-enzyme H_2O_2 sensor and an amperometric sarcosine biosensor based on the Pt-Fe_3O_4@C nanomaterials were prepared, respectively. Fig.2a shows the CV curves of the Fe_3O_4 modified GCE (Fe_3O_4/GCE), the Pt-Fe_3O_4 modified GCE (Pt-Fe_3O_4/GCE), the Pt-Fe_3O_4@PANI modified GCE (Pt-Fe_3O_4@PANI/GCE) and the Pt-Fe_3O_4@C modified GCE (Pt-Fe_3O_4@C/GCE) at the potential ranges from -0.4 to 0.8 V with a sweep rate of 50 $mV \cdot s^{-1}$ in the solution of 5 mM potassium ferricyanide. The CV curves of the GCE and the SOx/Pt-Fe_3O_4@C/GCE are also displayed in Fig. 2a as a comparation. Reversible redox behavior was detected on all the above electrodes. The CV curve of the Pt-Fe_3O_4@C/GCE shows the highest response signal in comparison with the CV curves of the bare GCE, Fe_3O_4/GCE, Pt-Fe_3O_4/GCE, and Pt-Fe_3O_4@PANI/GCE. In addition, the potential difference between the oxidation and the reduction peak current of the Pt-Fe_3O_4@C/GCE is the smallest. Consider these signals, it is clear that the Pt-Fe_3O_4@C/GCE electrode has the best electrochemical performance. The oxidation peak and the reduction peak current of the SOx/Pt-Fe_3O_4@C/GCE and the Pt-Fe_3O_4@PANI/GCE were reduced greatly because of the insulating films of SOx or PANI blocked the transfer of electrons. The interface properties of the modified electrode also was studied by electrochemical impedance spectroscopy (EIS). The EIS curves of the Pt-Fe_3O_4@C/GCE, the bare GCE, and the Pt-Fe_3O_4/GCE

in 10 mM of $K_3Fe(CN)_6^{3-}$ solution was illustrated in the inset of Fig. 2a. The electron transfer resistance (Ret) of the modified electrode was evaluated. The Pt-Fe_3O_4@C/GCE exhibits much smaller semicircular domains (26.1 Ω) than the bare GCE (757.6 Ω) and the Pt-Fe_3O_4/GCE (275.5Ω). EIS results further confirmed that Pt-Fe_3O_4@C has excellent electrochemical properties. These remarkable properties could be attributed to the conductivity and stability of the graphite carbon formed during the sample preparation process[39].

Fig. 2b illustrates the CV curves of Pt-Fe_3O_4@C/GCE in 5 mM $K_3Fe(CN)_6^{3-}$ solution with various sweep rates. It can be seen that both the anode peak potential and the cathode peak potential remained reversible and very little shift with the increase of sweep rate, showing the electrode has fast electron transfer kinetics and excellent electrochemical reaction ability. The relationship between the sweep rate and the anode and cathode peak currents is shown in the inset of Fig.2b. Both the cathode and the anode peak current increase monotonously with the sweep rate. In the range of 10 - 60 $mV{\cdot}s^{-1}$, the peak current and the square root of the sweep rates has a linear relationship, which showing a diffusion-controlled process of Pt-Fe_3O_4@C/GCE electrode. This also illustrates that the electrochemical reaction on the electrode is very fast. Fig. 2c shows the i-t response curves of the H_2O_2 on the bare GCE, the Fe_3O_4/GCE, the Pt-Fe_3O_4/GCE, the Pt-Fe_3O_4@PANI/GCE, and the Pt-Fe_3O_4@C/GCE in 0.1 M PBS with an applied potential of 0.3 V. With the continuously addition of 1 mM of H_2O_2, the response currents of all the electrodes increased accordingly. From fig. 2c, it can be seen that the response current of the Pt-Fe_3O_4@C/GCE is obviously higher than Pt-Fe_3O_4/GCE and other electrodes, showing that the Pt-Fe_3O_4@C nanomaterials have excellent catalytic ability towards H_2O_2. Further more, the response current of Pt-Fe_3O_4@C/GCE varies rapidly with the addition of hydrogen peroxide, and the response time is less than 2 s, as shown in fig. 2d. The upper inset in fig. 2d shows the linear fitting curve of the Pt-Fe_3O_4@C/GCE towards H_2O_2. It has a wider detection range of 0.001 - 6.0 mM with a linear regression equation of i/μA =0.74+19.16 c/mM, n = 32, R^2=0.994. The sensitivity is as high as 19.16 $\mu A{\cdot}mM^{-1}$ (271 $\mu A{\cdot}mM^{-1}{\cdot}cm^{-2}$). The lower inset shows the enlarged view of 0 - 0.03 mM H_2O_2. The Pt-Fe_3O_4@C/GCE has a lower LOD (0.6 μM) towards H_2O_2 and could be used as a high performance enzyme free H_2O_2 sensor.

[Fig. 2]

3.3 Electrochemical properties of the sarcosine biosensor

We further measured the electrochemical properties of SO_X/Pt-Fe_3O_4@C/GCE by using i-t method. During the test, a certain amount of sarcosine solution was dropped into the PBS solution each 100 s. With the increase of sarcosine concentration, the corresponding response current increased rapidly, indicating that the enzyme was successfully immobilized on the surface of Pt-Fe_3O_4@C electrode and the biosensor had a sensitive reaction speed toward sarcosine. The current response of SOx/Pt-Fe_3O_4@C/GCE toward sarcosine in 0.1 M PBS was recorded by keeping the potential at 0.3 V. The responds current of sarcosine is in a linear range between 0.5 to 60 μM. The regression linear fitting equation is: i/nA = 3.45 c/μM + 7.18, R^2=0.995. According to the calibration curve, it is estimated that the LOD of the sarcosine biosensor is 0.43 μM according to S/N = 3. These values are comparable to the behaviors of the recent reported sarcosine sensors (Table1).

[Fig. 3]

[Table 1]

Anti-interference response is a great challenge for sarcosine analysis, because sarcosine concentration is lower than many electrochemical activity interference in serum. Maltose (Mal), Citric acid (CA), Fructose (Fru), K^+, Ca^{2+}, Dop, UA, AA, and Cysteine (Cys) coexist with sarcosine in human blood serum. The anti-interference performance of SOx/Pt-Fe_3O_4@C/GCE toward these interfering species was evaluated by using i-t measurement. The current responses of the SOx/Pt-Fe_3O_4@C/GCE biosensor in 0.1 M PBS with continuously adding sarcosine (50 μM), Mal (300 μM), CA (300 μM), Fru (300 μM), K^+ (300 μM), Ca^{2+} (300 μM), AA (100 μM), Dop (100 μM), UA (300 μM) and Cys (300 μM) was shown in Fig.4. It can be clearly seen that SOx/Pt-Fe_3O_4@C/GCE has rapid response to sarcosine, while the response to interfering species can be neglected. This is due to the anti-interference ability of CS film[40]. These results demonstrate the superior selectivity of SOx/Pt-Fe_3O_4@C/GCE toward sarcosine. The biosensor was kept at 4 ℃ with plastic wrap when not in use. The long term stability of the sensor was also tested. The current signal could retain 90% of its initial data within 30 days, showing good stability.

[Fig. 4]

3.4 Detection of sarcosine in serum

In order to prove the accuracy of the SOx/Pt-Fe_3O_4@C/GCE biosensor in the analysis of sarcosine, standard addition method was used to detect sarcosine in human serum (diluted 10 times with PBS solution). The added concentration of the sarcosine was 10, 20 and 30 μM, respectively. Five repetitive experiments were carried out to calculate the precision of the sarcosine sensor. The relative standard deviation (RSD) of the determination is between 0.15 - 3.3%, as shown in table 2. At lower concentration (10 μM), the RSD is only 0.15%. While at higher concentration (20 or 30 μM), the RSD is a little larger than 3%, showing very high precision of the biosensor. The recovery rate of the biosensor is between 92-99%, showing high accuracy of the sensor. These results also show that the SO_X/Pt-Fe_3O_4@C/GCE biosensor may be used for actual sample testing.

[Table 2]

4. Conclusion

In summary, Pt-Fe_3O_4@C nanocomposites with high catalytic performance but lower Pt content (1.1 wt%) was prepared successfully. The presence of hollow magnetic material Fe_3O_4 makes the nanocomposites more convenient for recycling and more biocompatible. The formation of carbon via pyrolyzing polyaniline achieves excellent electron transfer ability and helps to keep the high catalytic activity of Pt. The prepared SOx/Pt-Fe_3O_4@C/GCE sarcosine biosensor has excellent sensing properties. The linear detection range of the sarcosine biosensor is 0.5 - 60 μM and the LOD is 0.43 μM, which is comparable to the content of sarcosine in serum or urine of prostate cancer patient. This biosensor has potential to be used in the large-scale screening of prostate cancer. The Pt-Fe_3O_4@C nanocomposites also could construct biosensors for other low concentration substrates in the field of medical and food safety.

Acknowledgments

The authors appreciate the financial support from the Shenzhen Science and Technology Innovation Commission (Grant No. JCYJ20180305124343508). This work was also supported by the leading

talents of Guangdong province program (2016LJ06N507), and the National Key Research and Development Program of China (2018YFB0704100).

Reference:

[1] A. Sreekumar, L.M. Poisson, T.M. Rajendiran, A.P. Khan, Q. Cao, J.D. Yu, B. Laxman, R. Mehra, R.J. Lonigro, Y. Li, M.K. Nyati, A. Ahsan, S. Kalyana-Sundaram, B. Han, X.H. Cao, J. Byun, G.S. Omenn, D. Ghosh, S. Pennathur, D.C. Alexander, A. Berger, J.R. Shuster, J.T. Wei, S. Varambally, C. Beecher, A.M. Chinnaiyan, Metabolomic profiles delineate potential role for sarcosine in prostate cancer progression, Nature 457 (2009) 910-914.

[2] B. Bickers, H.C. Aukim, New molecular biomarkers for the prognosis and management of prostate cancer--the post PSA era, Anticancer Res. 29 (2009) 3289-3298.

[3] N. Gray, R. Zia, A. King, V.C. Patel, J. Wendon, M.J.W. McPhail, M. Coen, R.S. Plumb, I.D. Wilson, J.K. Nicholson, High-speed quantitative UPLC-MS analysis of multiple amines in human plasma and serum via precolumn derivatization with 6-Aminoquinolyl-N-hydroxysuccinimidyl carbamate: Application to acetaminophen-induced liver failure, Anal. Chem. 89 (2017) 2478-2487.

[4] Y. Jiang, X. Cheng, C. Wang, Y. Ma, Quantitative Determination of sarcosine and related compounds in urinary samples by liquid chromatography with Tandem Mass Spectrometry, Anal. Chem. 82 (2010) 9022-9027.

[5] N. Tin Phan, P. Toan Van, D.T.N. Tram, K. Eersels, P. Wagner, T.T.N. Lien, Development of an impedimetric sensor for the label-free detection of the amino acid sarcosine with molecularly imprinted polymer receptors, Sensor. Actuat. B-Chem. 246 (2017) 461-470.

[6] Z. Xue, H. Wang, H. Rao, N. He, X. Wang, X. Liu, X. Lu, Amperometric indicator displacement assay for biomarker monitoring: Indirectly sensing strategy for electrochemically inactive sarcosine, Talanta 167 (2017) 666-671.

[7] J. Hu, W. Wei, S. Ke, X. Zeng, P. Lin, A novel and sensitive sarcosine biosensor based on organic electrochemical transistor, Electrochim. Acta 307 (2019) 100-106.

[8] X. Y. Jiang, L. Zhang, Y. L. Liu, X. D. Yu, Y. Y. Liang, P. Qu, et al., Hierarchical CuInS2-based heterostructure: Application for photocathodic bioanalysis of sarcosine, Biosens. Bioelectron. 107 (2018) 230-236.

[9] Q. Wang, C. Yang, Q. G. Yang, S. H. Yu, H. P. Yang, Platinum-loaded mesoporous nickel phosphonate and its electrochemical application for sarcosine detection, Anal. Chim. Acta 1046 (2019) 93-98.

[10 I. A. Alaton, I. A. Balcioglu, D. W. Bahnemann, Advanced oxidation of a reactive dyebath effluent: Comparison of O3, H2O2/UV-C and TiO2/UV-A processes, Water Res. 36 (2002) 1143-1154.

[11] Q. Chen, L. Z. Feng, J. J. Liu, W. W. Zhu, Z. L. Dong, Y. F. Wu, Z. Liu, Intelligent Albumin-MnO2 nanoparticles as pH-/H2O2-responsive dissociable nanocarriers to modulate tumor hypoxia for effective combination therapy, Adv. Mater. 28 (2016) 7129-7136.

[12] Y. X. Lin, Q. Zhou, D. P. Tang, R. Niessner, D. Knopp, Signal-On photoelectrochemical immunoassay for aflatoxin B1 based on enzymatic product-etching MnO2 nanosheets for dissociation of carbon dots, Anal. Chem. 89 (2017) 5637-5645.

[13] M. Sundaresan, Z.X. Yu, V.J. Ferrans, K. Irani, T. Finkel, Requirement for generation of H2O2for platelet derived growth factor signal transduction, Science 270 (1995) 296-299.

[14] F. Yang, L. Zhao, B. Gao, X. Y. Xu, X. D. Cao, The interfacial behavior between biochar and soil minerals and its effect on biochar stability, Environ. Sci. Technol. 50 (2016) 2264-2271.

[15] B. Ma, C. Kong, X. Hu, K. Liu, Q. Huang, J. Lv, et al., A sensitive electrochemical

nonenzymatic biosensor for the detection of H2O2 released from living cells based on ultrathin concave Ag nanosheets, Biosens. Bioelectron. 106 (2018) 29-36.
[16] T. S. C. R. Rebelo, C. M. Pereira, M. G. F. Sales, J. P. Noronha, J. Costa-Rodrigues, F. Silva, M. H. Fernandes, Sarcosine oxidase composite screen-printed electrode for sarcosine determination in biological samples, Anal. Chim. Acta 850 (2014) 26-32.
[17] J. Li, J. Ma, Y. Zhang, Z. Zhang, G. He, An amperometric biosensor for the assay of sarcosine based on the cross coupled chemical and electrochemical reactions with practical applications, J. Electroanal. Chem. 833 (2019) 568-572.
[18] H. P. Yang, J. J. Wang, C. Yang, X. L. Zhao, S. H. Xie, Z. C. Ge, Nano Pt@ZIF8 modified electrode and its application to detect sarcosine, J. Electrochem. Soc. 165 (2018) H247-H250.
[19] P. Kumar, V. Narwal, R. Jaiwal, C.S. Pundir, Construction and application of amperometric sarcosine biosensor based on SOxNPs/AuE for determination of prostate cancer, Biosens. Bioelectron. 122 (2018) 140-146.
[20] A.D. Chowdhury, A.B. Ganganboina, Y.C. Tsai, H.C. Chiu, R.A. Doong, Multifunctional GQDs-Concanavalin A@Fe3O4 nanocomposites for cancer cells detection and targeted drug delivery, Anal. Chim. Acta, 1027 (2018) 109-120.
[21] Z. M. Fu, B. W. Yang, Y. Zhang, N. Zhang, Z. X. Yang, Dopant segregation and CO adsorption on doped Fe3O4 (111) surfaces: A first-principle study, J. Catal. 364 (2018) 291-296.
[22] A. Nakhaei, A. Davoodnia, S. Yadegarian, Nano-Fe3O4@ZrO2-SO3H as highly efficient recyclable catalyst for the green synthesis of fluoroquinolones in ordinary or magnetized water, Iranian J. Catal. 8 (2018) 47-52.
[23] H. Wang, X. L. Zhao, X. J. Han, Z. Tang, F. H. Song, S. Y. Zhang, Y. R. Zhu, W. J. Guo, Z. Q. He, Q. W. Guo, F. C. Wu, X. G. Meng, J. P. Giesy, Colloidal stability of Fe3O4 magnetic nanoparticles differentially impacted by dissolved organic matter and cations in synthetic and naturally-occurred environmental waters, Environ. Pollut. 241 (2018) 912-921.
[24] Y. Y. Wang, X. J. Liu, G. Y. Deng, Q. Wang, L. J. Zhang, Q. G. Wang, J. Lu, J. Mater, Multifunctional PS@CS@Au-Fe3O4-FA nanocomposites for CT, MR and fluorescence imaging guided targeted-photothermal therapy of cancer cells, J. Mater. Chem-B 5 (2017) 4221-4232.
[25] Z. S. Wu, S. B. Yang, Y. Sun, K. Parvez, X. L. Feng, K. Mullen, 3D nitrogen-doped graphene Aerogel-supported Fe3O4 nanoparticles as efficient eletrocatalysts for the oxygen reduction Reaction, J. Am. Chem. Soc. 134(2012) 9082-5.
[26] X. L. Zhao, Z. H. Li, C. Chen, Y. H. Wu, Z. G. Zhu, H. L. Zhao, M.B. Lan, A novel biomimetic hydrogen peroxide biosensor based on Pt flowers-decorated Fe3O4/graphene nanocomposite, electroanal. 29 (2017) 1518-1523.
[27] M.B. Gawande, P. S. Branco, R. S. Varma, Nano-magnetite (Fe3O4) as a support for recyclable catalysts in the development of sustainable methodologies, Chem. Soc. Rev. 42 (2013) 3371-3393.
[28] M. Antonietti, E. Wenz, L. Bronstein, M. Seregina, Synthesis and characterization of noble metal colloids in block copolymer micelles, Adv. Mater. 7(1995) 1000-1005.
[29] X. H. Huang, I. H. El-Sayed, W. Qian, M. A. El-Sayed, Cancer cell imaging and photothermal therapy in the near-infrared region by using gold nanorods, J. Am. Chem. Soc. 128 (2006) 2115-2120.
[30] J. J. Zhang, F. F. Cheng, J. J. Li, J. J. Zhu, Y. Lu, Fluorescent nanoprobes for sensing and imaging of metal ions: Recent advances and future perspectives, Nano Today 11 (2016) 309-329.
[31] M.S. Kim, S. H. Kweon, S. Cho, S. An, M. I. Kim, J. Doh, J. Lee, Pt-decorated magnetic

nanozymes for facile and sensitive point-of-care bioassay, Acs. Appl. Mater. Interfaces. 9 (2017) 35133-35140.
[32] D. Gou, G. Xie, Y. Li, X. Zhang, H. Chen, Voltammetric immunoassay for Mycobacterium tuberculosis secretory protein MPT64 based on a synergistic amplification strategy using rolling circle amplification and a gold electrode modified with graphene oxide, Fe3O4 and Pt nanoparticles, Microchim. Acta 185 (2018) 436-445.
[33] D. Chovan, M. Nolan, S.A.M. Tofail, First principles simulations of elastic properties of radiopaque NiTiPt, J. Alloys. Compd. 630 (2015) 54-59.
[34] R. Cuadrado, T.J. Klemmer, R.W. Chantrell, Magnetic anisotropy of Fe1-yXyPt-L1(0) X = Cr, Mn, Co, Ni, Cu bulk alloys, Appl. Phys. Lett. 105 (2014) 4.
[35] N. Moghimi, M. Mohapatra, K. T. Leung, Bimetallic nanoparticles for arsenic detection, Anal. Chem. 87 (2015) 5546-5552.
[36] Q. W. Tang, H. H. Zhang, Y. Y. Meng, B. L. He, L. M. Yu, Dissolution engineering of platinum alloy counter electrodes in Dye-Sensitized solar cells, Angew. Chem-Int Edit 54 (2015) 11448-11452.
[37] X. Y. Chen, Z. J. Zhang, X. X. Li, C. W. Shi, Hollow magnetite spheres: Synthesis, characterization, and magnetic properties, Chem. Phys. Lett. 422 (2006) 294-298.
[38] Q. G. Yang, C. Yang, Q. Wang, F. Yang, C. Y. Song, H. P. Yang, Electrochemical biosensor based on nano TiO2 loaded with highly dispersed photoreduced nano platinum, J. Electrochem. Soc. 165 (2018) B610-B615.
[39] J. Li, M. Chen, D. A. Cullen, S. Hwang, M. Wang, B. Li, K. Liu, S. Karakalos, M. Lucero, H. Zhang, C. Lei, H. Xu, G.E. Sterbinsky, Z. Feng, D. Su, K.L. More, G. Wang, Z. Wang, G. Wu, Atomically dispersed manganese catalysts for oxygen reduction in proton-exchange membrane fuel cells, Nat. Catal. 1 (2018) 935-945.
[40] P. Sorlier, A. Denuziere, C. Viton, A. Domard, Relation between the degree of acetylation and the electrostatic properties of chitin and chitosan, Biomacromolecules, 2 (2001) 765-772.
[41] M. J. Pannell, E. E. Doll, N. Labban, M. B. Wayu, J. A. Pollock, M. C. Leopold, Versatile sarcosine and creatinine biosensing schemes utilizing layer-by-layer construction of carbon nanotube-chitosan composite films, J. Electroanal. Chem. 814 (2018) 20-30.
[42] U. Lad, G.M. Kale, R. Bryaskova, Sarcosine oxidase encapsulated polyvinyl Alcohol-Silica-AuNP hybrid films for sarcosine sensing electrochemical bioelectrode, J. Electrochem. Soc. 161 (2014) B98-B101.

Scheme 1. The fabrication process and the mechanism of the SOx/Pt-Fe_3O_4@C/GCE biosensor.

Table 1. Comparison of sensing performances of SOx/Pt-Fe_3O_4@C/GCE with other electrochemical sarcosine sensors.

Table 2. The standard recovery of the sarcosine sensor in serum sample.

Figure Captions

Fig. 1. a) SEM, b, c) TEM, d) elemental mapping and e) element analysis spectrum, f) selected area electron diffraction pattern of Pt-Fe_3O_4@C nano composites.

Fig. 2. a) CVs of Pt-Fe_3O_4@C/GCE, Pt-Fe_3O_4@PANI/GCE, Pt-Fe_3O_4/GCE, Fe_3O_4/GCE, bare GCE and SOx/Pt-Fe_3O_4@C/GCE at a sweep rate of 0.05 V s^{-1} in 5 mM $K_3Fe(CN)_6^{3-}$ solution, and the EIS of Pt-Fe_3O_4@C/GCE, bare GCE, Pt-Fe_3O_4/GCE in 10 mM $K_3Fe(CN)_6^{3-}$ solution, b) CVs of the Pt-Fe_3O_4@C/GCE in 5 mM $K_3Fe(CN)_6^{3-}$ solution at sweep rates from 0.01 to 0.06 V s^{-1}. The linear relationship between the redox peak current is shown in the illustration, c) I-T curves of Pt-Fe_3O_4/GCE, Pt-Fe_3O_4@PANI/GCE, Pt-Fe_3O_4@C/GCE, Fe_3O_4/GCE and the GCE to the successive addition of 1mM H_2O_2, in 0.1 M PBS (PH=7.0) at 0.3 V potential, d) I-T curves of Pt-Fe_3O_4@C/GCE to the successive addition of H_2O_2 in 0.1 M PBS (PH=7.0) at 0.3 V. Insets including corresponding calibration plot of the hydrogen peroxide sensor at 0-6mM and an enlarged view of 0-0.03 mM H_2O_2.

Fig. 3. I-T curves of SOx/Pt-Fe_3O_4@C/GCE to continuous addition of sarcosine. The inset shows the linear plot for the SOx/Pt-Fe_3O_4@C/GCE and the enlarged view of 0-2 μM of sarcosine.

Fig. 4. The anti-interference performance of Pt-Fe_3O_4@C/GCE for Mal, CA, Fru, K^+, Ca^{2+}, AA, UA, Dop, and Cys.

Scheme 1.

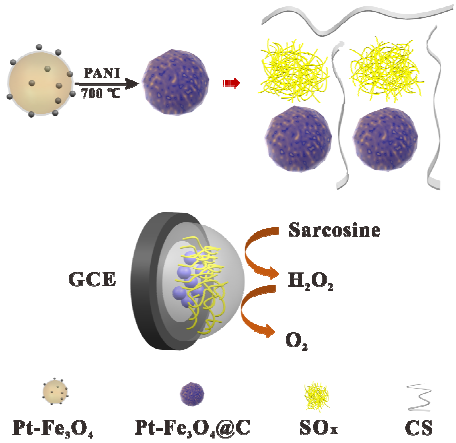

Table 1.

electrodes	linear range (μM)	limit of detection (μM)	potential (V)	interference study					ref
				CA	AA	UA	Dop	Cys	
Pt/MNP/ GCE	5-40	0.24	0.4	No	No	No	No	No	[9]
Carbon screen printed electrodes	0.01-0.1	0.016	0.6	-	-	-	-	-	[16]
PAA /GCE	0.001-0.05 (logarithmic)	0.0004	-0.55	-	No	No	-	-	[17]
Pt@ZIF8/GCE	5-30	1.06	0.4	No	Yes	No	-	Yes	[18]
Au	0.1-100	0.01	1	No	No	No	-	-	[19]
CNT/Pt	6-750	6	0.2	-	-	No	-	-	[41]
PVA-Au-pph TEOS -SOD- GE	500-7500	500	0.55	-	-	-	-	-	[42]
Pt-Fe_3O_4@C/GCE	0.5-60	0.43	0.3	No	No	No	No	No	this work

No, represents noninterference; Yes, represents interference; -, represents the interference test was not performed.

Table 2.

No.	Added (μM)	Found (μM)	Recovery (%)	RSD (%)
1	10.0	9.9	99	0.15
2	20.0	19.0	95	3.1
3	30.0	27.6	92	3.3

Fig.1.

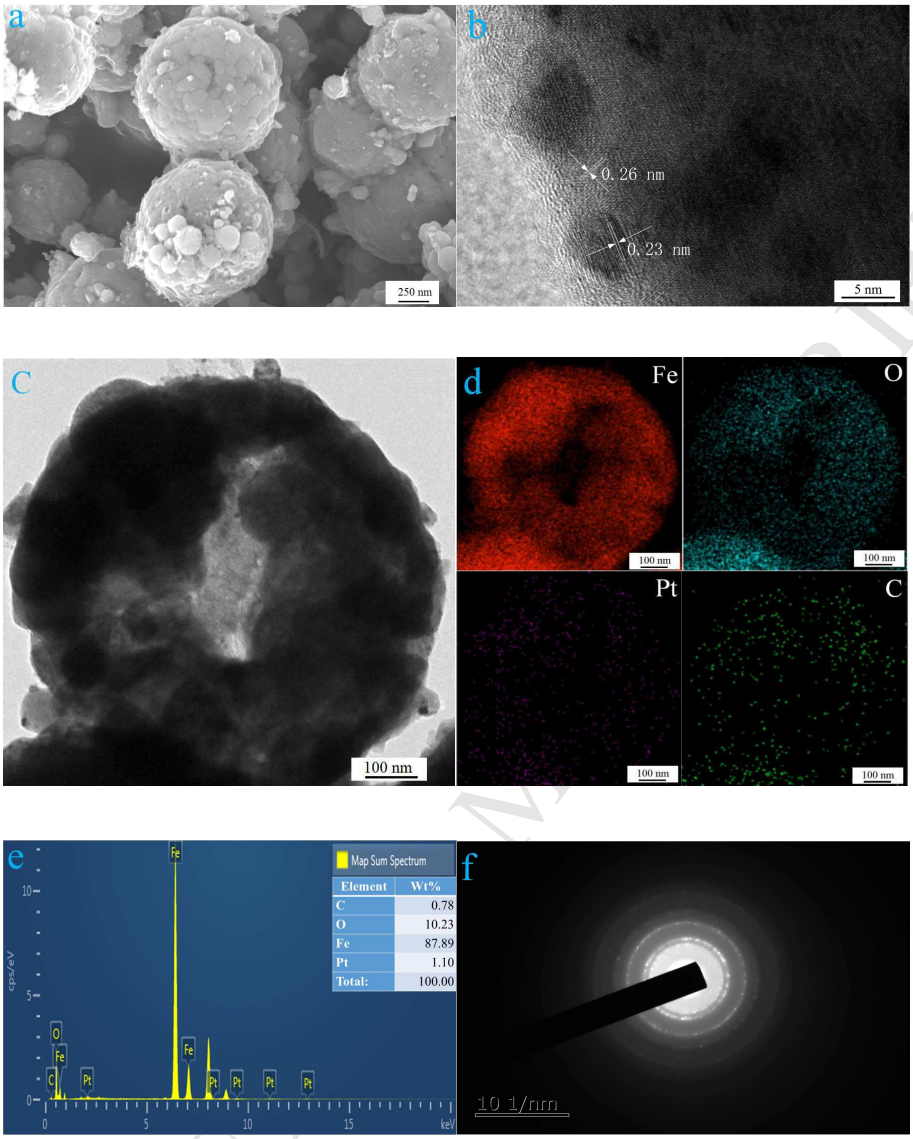

Fig.2.

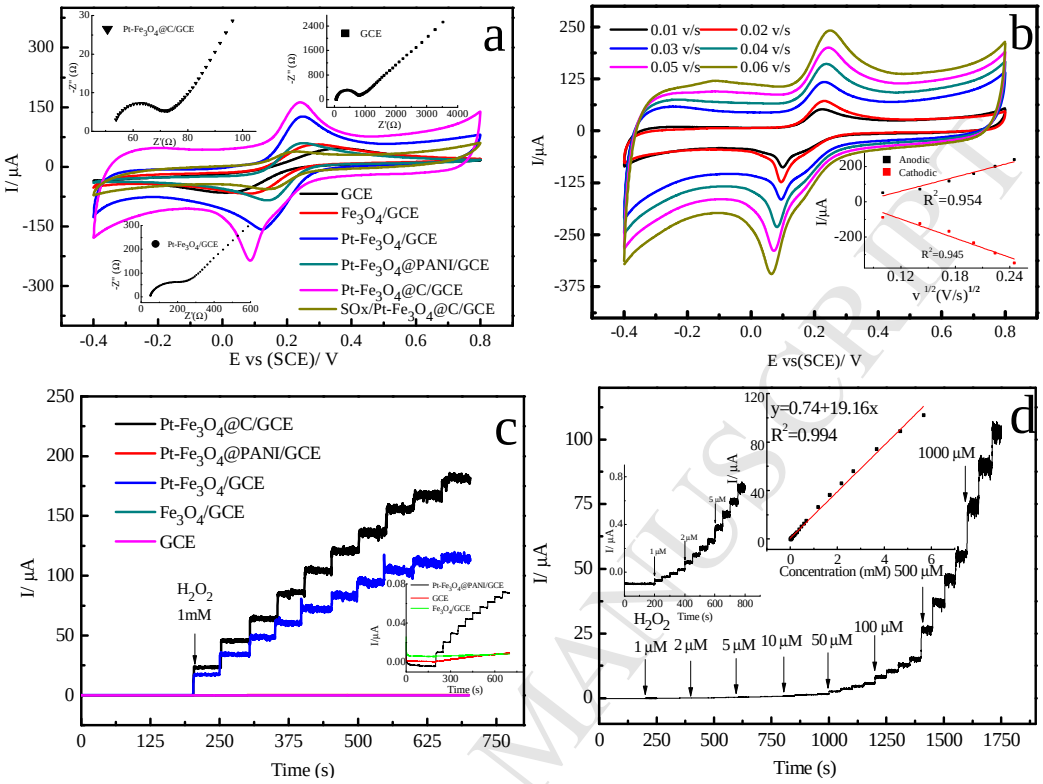

Fig.3.

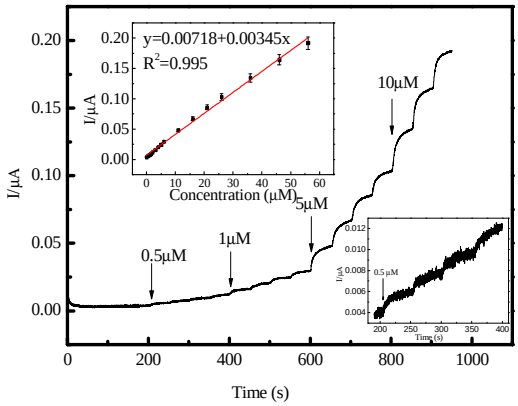

Fig.4

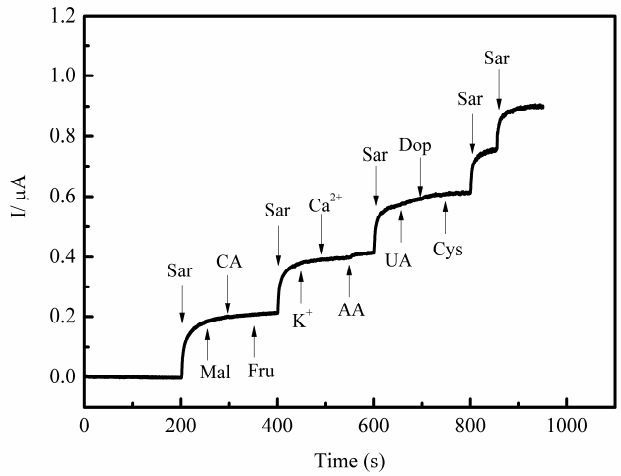

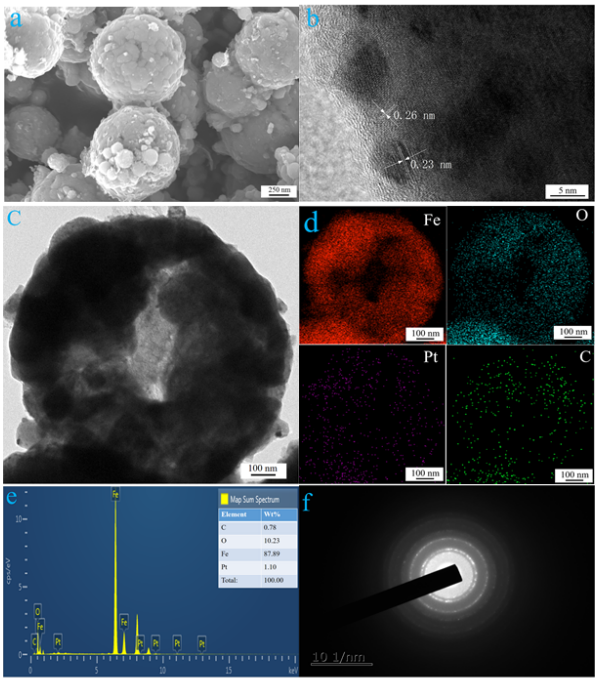

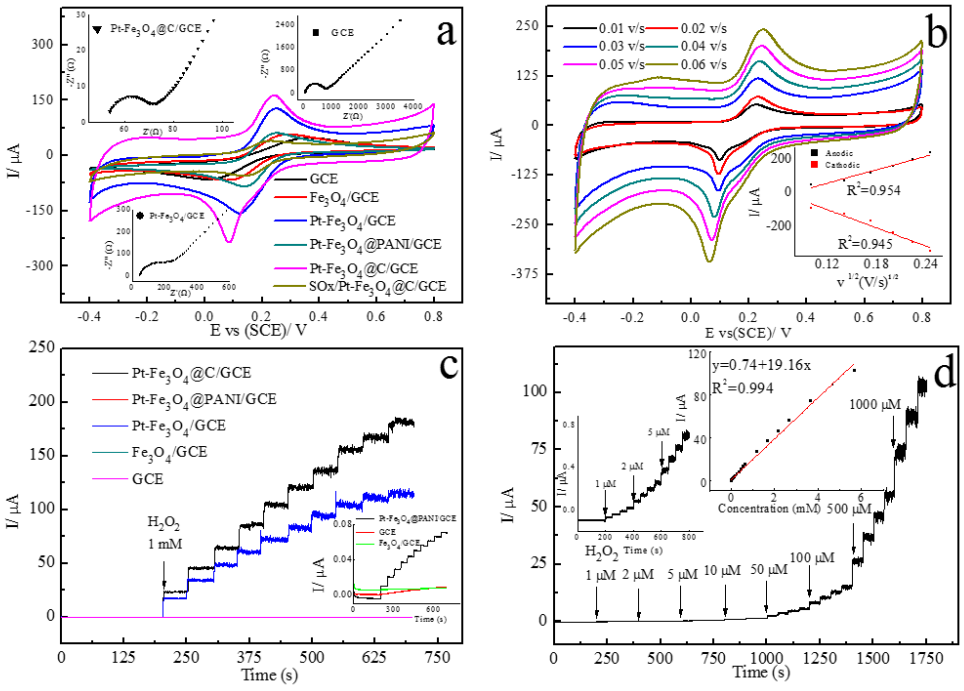

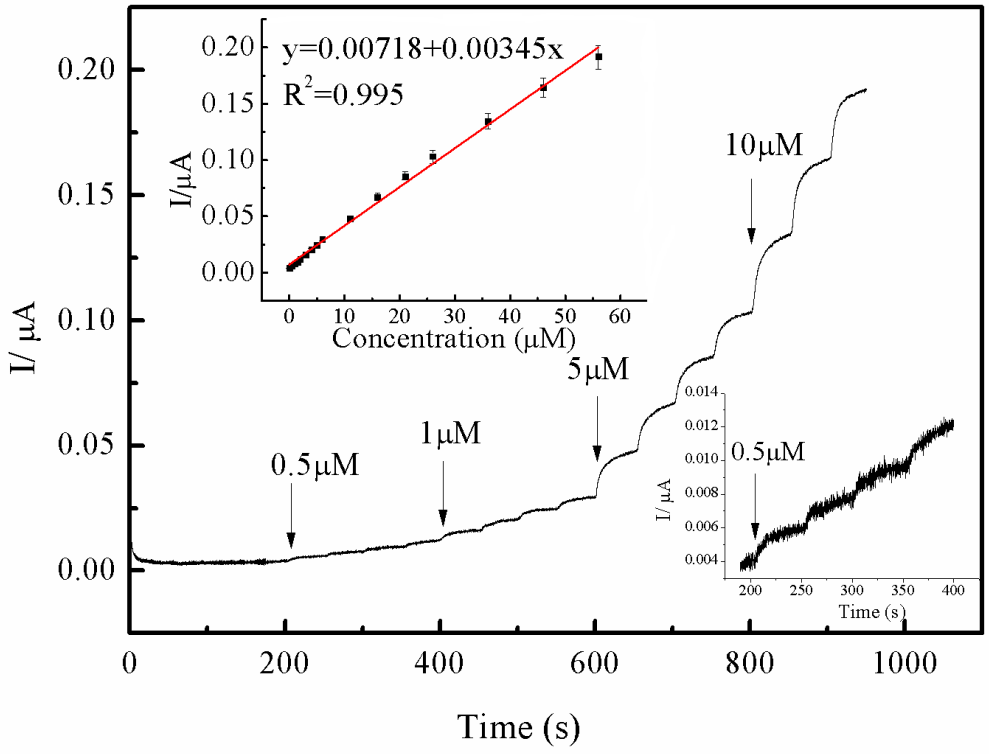

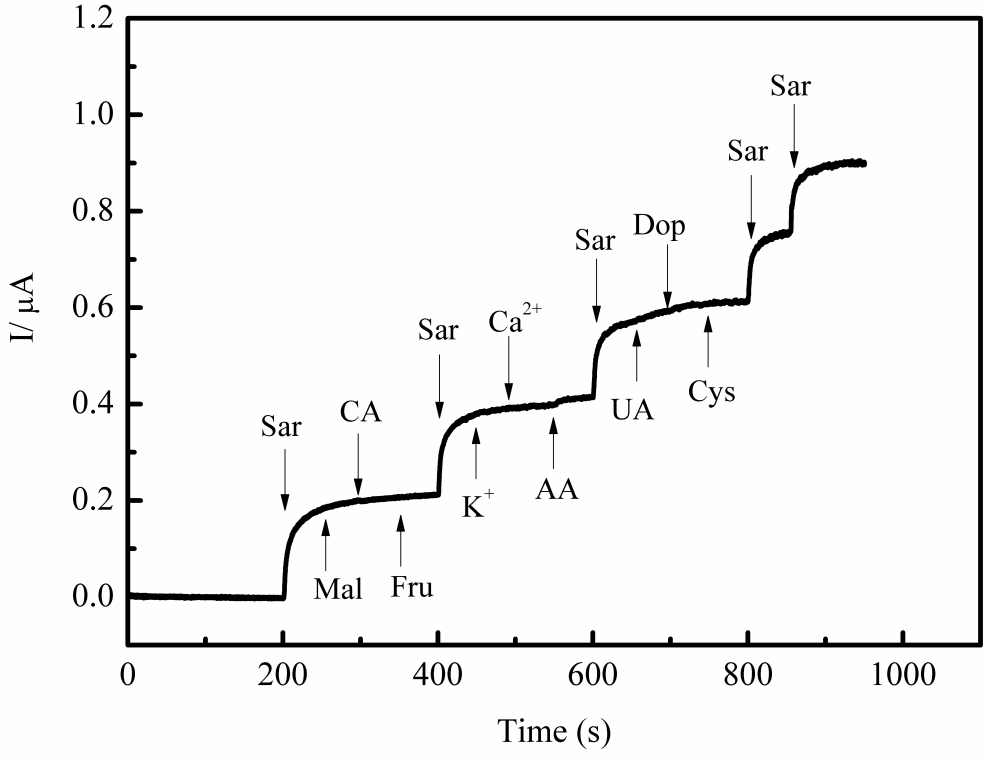

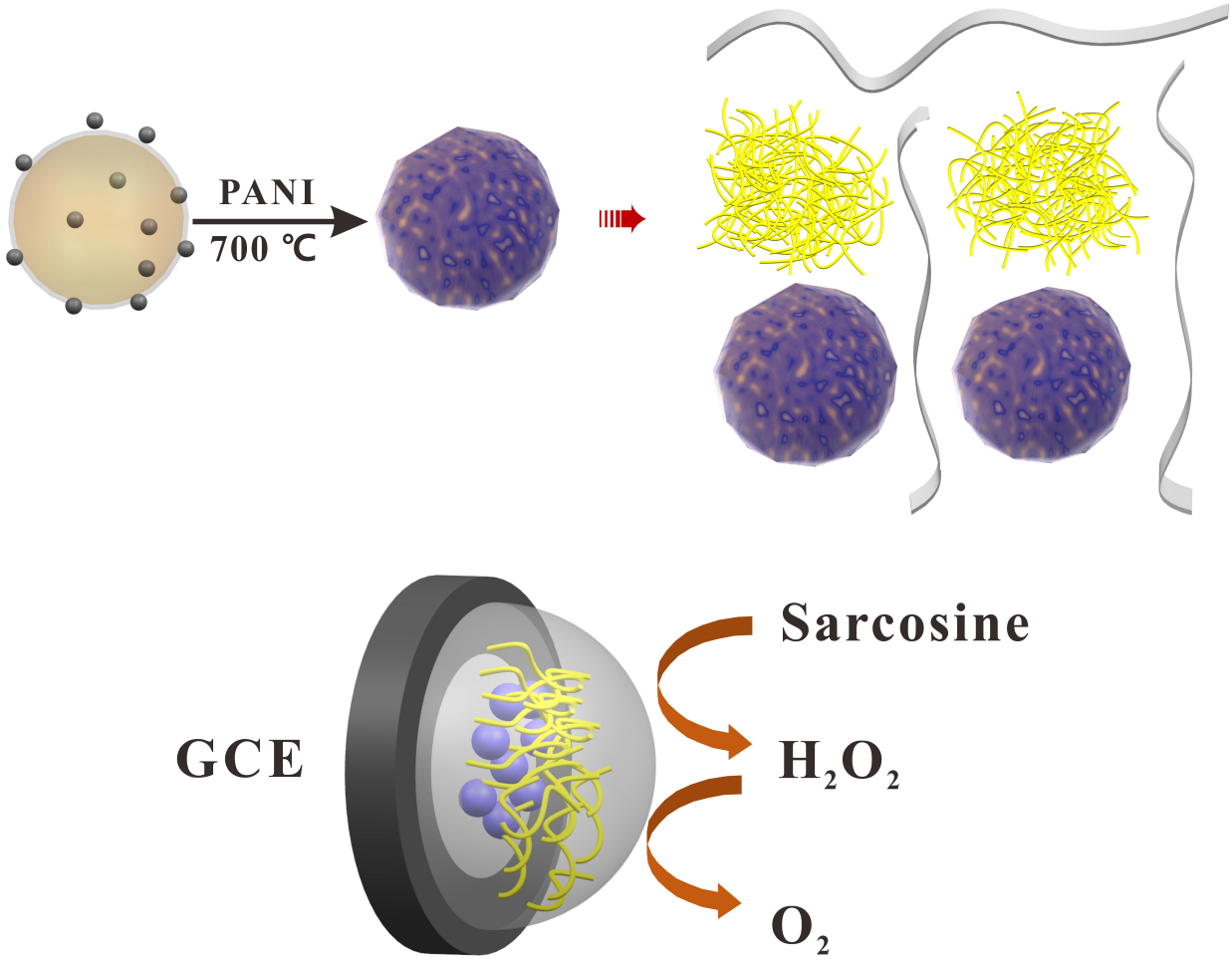
PANI
700 ℃
GCE
Sarcosine
H_2O_2
O_2
$Pt\text{-}Fe_3O_4$
$Pt\text{-}Fe_3O_4@C$
SO_x
CS

- Hollow Pt-Fe_3O_4@C nanospheres with high catalytic activity were prepared.
- The SOx/Pt-Fe_3O_4@C/GCE biosensor has good sensing properties towards sarcosine.
- The sensor has a linear range of 0.5-60 μM with good anti-interference property.

Declaration of interests

☒ The authors declare that they have no known competing financial interests or personal relationships that could have appeared to influence the work reported in this paper.

☐The authors declare the following financial interests/personal relationships which may be considered as potential competing interests:

There is no conflict of interests.